BBA - Biomembranes 1861 (2019) 1510–1521

Contents lists available at ScienceDirect

BBA - Biomembranes

journal homepage: www.elsevier.com/locate/bbamem

Characterization of the interaction of the antifungal and cytotoxic cyclic glycolipopeptide hassallidin with sterol-containing lipid membranes

Anu Humisto[a], Jouni Jokela[a], Knut Teigen[b], Matti Wahlsten[a], Perttu Permi[c,d], Kaarina Sivonen[a], Lars Herfindal[e,*]

[a] Department of Microbiology, University of Helsinki, Viikki Biocenter 1, P.O. Box 56, FI-00014 Helsinki, Finland
[b] Centre for Pharmacy, Department of Biomedicine, University of Bergen, N-5009 Bergen, Norway
[c] Department of Biological and Environmental Science, University of Jyvaskyla, P.O Box 35, FI-40014 Jyvaskyla, Finland
[d] Department of Chemistry, Nanoscience Center, University of Jyvaskyla, P.O Box 35, FI-40014 Jyvaskyla, Finland
[e] Centre for Pharmacy, Department of Clinical Science, University of Bergen, N-5009 Bergen, Norway

ARTICLE INFO

Keywords:
Anabaena
Candida albicans
Cyanobacteria
Mammalian cells
Mechanism
Membrane
Cholesterol
Lipopeptide

ABSTRACT

Hassallidins are cyclic glycolipopeptides produced by cyanobacteria and other prokaryotes. The hassallidin structure consists of a peptide ring of eight amino acids where a fatty acid chain, additional amino acids, and sugar moieties are attached. Hassallidins show antifungal activity against several opportunistic human pathogenic fungi, but does not harbor antibacterial effects. However, they have not been studied on mammalian cells, and the mechanism of action is unknown. We purified hassallidin D from cultured cyanobacterium *Anabaena* sp. UHCC 0258 and characterized its effect on mammalian and fungal cells. Ultrastructural analysis showed that hassallidin D disrupts cell membranes, causing a lytic/necrotic cell death with rapid presence of disintegrated outer membrane, accompanied by internalization of small molecules such as propidium iodide into the cells. Furthermore, artificial liposomal membrane assay showed that hassallidin D selectively targets sterol-containing membranes. Finally, *in silico* membrane modeling allowed us to study the interaction between hassallidin D and membranes in detail, and confirm the role of cholesterol for hassallidin-insertion into the membrane. This study demonstrates the mechanism of action of the natural compound hassallidin, and gives further insight into how bioactive lipopeptide metabolites selectively target eukaryotic cell membranes.

1. Introduction

Cyanobacteria produce a large spectrum of bioactive natural products, such as antimicrobial, antifungal, antiviral, or cytotoxic compounds [1–3]. Structurally diverse bioactive compounds from cyanobacteria are produced through ribosomal, nonribosomal, or hybrid pathways and include compounds such as peptides, polyketides, terpenes, and lipopeptides. Novel compounds are constantly identified through bioactivity-guided methods and genome mining. Despite the vast number of natural products described from cyanobacteria, the mechanisms of action of many bioactive compounds have been studied less extensively. However, information on the target and the mechanism are ecologically important and essential if compounds will also be evaluated for instance as pharmaceuticals or anti-fouling agents.

Lipopeptides are compounds with a fatty acid-derived moiety attached to the amino-acid fragment. A number of cyanobacterial bioactive compounds are lipopeptides with varying linear to cyclic structures [1]. Anabaenolysins, calophycins, laxaphycins, lobocyclamides, lyngbyacyclamides, muscotoxins, and puwainaphycins are all examples of cyclic lipopeptides extracted from cyanobacteria that exhibit cytotoxic or antifungal activities [4–10]. In addition, antifungal glycosylated cyclic lipopeptides known as hassallidins (A to E) are produced by cyanobacteria [11–14]. The hassallidin structure consists of a peptide ring of eight amino acids where one additional amino acid, fatty acid, and one to three sugar moieties are attached. Hassallidins have been found from cyanobacteria species *Anabaena*, *Aphanizomenon*, *Cylindrospermopsis*, *Nostoc*, *Planktothrix*, and *Tolypothrix* [11,13,14]. Hassallidin family members known as balticidins were described from *Anabaena cylindrica* [15]. Hassallidins have antifungal activities against opportunistic human pathogenic fungi, including *Candida*, *Aspergillus*, *Fusarium*, and *Penicillium* sp. [11–13,15,16]. Additionally, activity against human acute T cell leukemia (Jurkat ATCC-TIB-152) and murine aneuploid fibrosarcoma (L929) cells has been reported [16]. Hassallidins are produced through a nonribosomal peptide biosynthesis

* Corresponding author.
E-mail address: lars.herfindal@uib.no (L. Herfindal).

https://doi.org/10.1016/j.bbamem.2019.03.010
Received 26 August 2018; Received in revised form 15 February 2019; Accepted 15 March 2019
Available online 19 June 2019

pathway and the biosynthesis machinery was first described in *Anabaena* sp. 90 [13,17]. In a comparison study between hassallidin A and the structurally similar echinocandin antifungal caspofungin, the mechanism of action was hypothesized to involve the cell membrane [18].

Hassallidins are interesting molecules for research due to their strong antifungal activity and complicated structure. Here we have studied hassallidin D that was purified from the cyanobacterium *Anabaena* sp. UHCC 0258. We tested its activity against eukaryotic cells, including acute myeloid leukemia, normal rat kidney, and yeast cells. The ultrastructural and cellular functions on mammalian cells were studied to elucidate the mechanism of action. Furthermore, artificial membranes together with *in silico* modeling were used to determine the cellular target of hassallidin. This study presents the mechanism behind the cytotoxic activity of hassallidins, namely disruption of membranes containing sterols.

2. Materials and methods

2.1. Purification of hassallidin D

A previously identified hassallidin producer cyanobacterium *Anabaena* sp. UHCC 0258 (previously named as *Anabaena* sp. 258), isolated from Lake Tuusulanjärvi, Finland, was maintained in 40 ml liquid Z8X culture medium [19]. For hassallidin D purification, cells were grown in batches of 3 l Z8X media for approximately 30 days at a photo irradiance of 8 to 20 $\mu mol\, m^{-2}\, s^{-1}$ at 20 to 25 °C. Cells were collected by centrifugation for 10 min at 7000 × *g* and freeze dried. The purification of hassallidin was prepared following the previously published procedure with some modifications [13]. In one batch, 2 g of freeze-dried cyanobacterial biomass (1 g in two vials) were each dissolved in 35 ml acetonitrile (ACN):dimethyl sulfoxide (DMSO) (1:1) with a Silent Crusher M homogenizer (Heidolph, Germany) (30 s, 20000 rpm). The suspensions were centrifuged at 10000 × *g* for 5 min and supernatants were pooled into a round bottom flask. The pellets were extracted again with 25 ml ACN:DMSO (1:1) solution. Acetonitrile was evaporated from the solution in a round bottom flask with a rotary evaporator at 30 °C. The extraction was continued as described [13] by solid phase extraction (SPE) cartridges (Phenomenex Inc. Strata C18-E 5 g/20 ml, 55 µm, 70 Å). Hassallidin D was further purified with a semipreparative Luna C8 (2) 10 × 150 mm column with isocratic HPLC (Agilent 1100) runs. HPLC was combined with a mass spectrometer (LC/MSD trap XCT Plus, Agilent) to assess the correct peaks and the purity of the analytes (Supplementary Fig. S1). The collected peaks representing the four hassallidin variants were diluted in water (1:1) and passed through SPE cartridges (Phenomenex Inc. Strata C18-E 200 mg/6 ml, 55 µm, 70 Å). Hassallidin was eluted from the cartridges with 5 ml 90% aqueous ACN. Fractions were dried with a stream of nitrogen gas. The purity of hassallidin D was verified with QTOF (Waters LC-MS: Acquity I-Class-Synapt G2-Si) (Supplementary Fig. S1). Since some impurities were still found, we repeated the HPLC and SPE purification steps before freeze drying the isolated compounds. From a total of 15 g of dried cyanobacterial biomass, approximately 11 mg of hassallidin D (**2**) was purified. The yield of variant **1** was about 2 mg and variants **3** and **4** were 1 to 1.5 mg. Freeze-dried hassallidin D variants were dissolved in DMSO to prepare 5-mM stock solutions for use in experiments.

2.2. NMR analyses

NMR spectra of native hassallidin D (**2**) were recorded in DMSO-d_6 at 40 °C using a Bruker Avance III HD 850 MHz NMR spectrometer equipped with a 5-mm cryogenically cooled TCI probe head. ^{1}H spectra were acquired using 16,000 complex points, corresponding to an acquisition time of 0.96 s and accumulated with 4 transients. Homonuclear TOCSY and COSY spectra were accumulated with 8 transients, using 256 and 4096 complex points in F1 and F2 dimensions, corresponding to acquisition times of 15.1 ms and 241 ms in t1 and t2, respectively. The isotropic mixing time was 80 ms for TOCSY. Spectra of the heteronuclear multiple-bond correlation experiment (^{13}C-HMBC) was accumulated with 32 transients using 512 and 1536 complex points in F1 and F2, respectively. This translates to acquisition times of 5.4 ms and 90 ms in t1 and t2, respectively. A first-order J filter with 1JHC set to 140 Hz was used to remove one-bond H−C connectivities, whereas 8 Hz for establishing multiple-bond H−C correlations was used. A heteronuclear single quantum coherence experiment (^{13}C-HSQC) was acquired with 512 and 1024 complex points in t1 and t2 domains, corresponding to acquisition times of 5.3 and 60 ms, respectively.

Roughly 0.4 mg of hassallidin D (**2**) was hydrolyzed 1 h at 100 °C in 0.5 ml of 2 M D_2SO_4 in D_2O + DMSO-d_6 (9:1). Proton spectrum from this and the reference compounds D-Mannosamine hydrochloride (2 mg, Sigma-Aldrich, St. Louis, USA) and D-(+)-Galactosamine hydrochloride (2 mg, Sigma-Aldrich, St. Louis, USA) in the same solvent system were run according to Giner et al. [20].

2.3. Monosaccharide MS analysis

D- and L-Mannose were purchased from Sigma-Aldrich (St. Louis, USA). Hydrolysis of hassallidin D and sample derivatizations were done according to Wang et al. [21] with the following exceptions: About 0.4 mg of hassallidin D was hydrolyzed, freeze dried instead of drying under N_2-gas stream, and the reagents L-cysteine methyl ester (Sigma) and o-tolyl isothiocyanate (Thermo Fisher GmbH, Germany, instead of phenyl isothiocyanate) were added simultaneously, and reaction mixture was incubated at 60 °C for 1 h and diluted with MeOH before UPLC-QTOF analysis. Samples of 1 µl were analyzed with two LC-methods. The sample was injected to Kinetex C8 column (50 or 100 × 2 mm, 1.7 µm, Phenomenex Inc.), which was eluted 0.3 ml min^{-1} at 40 °C with 95% water (+0.1% HCOOH, eluent A) and 5% ACN:isopropanol (1:1, +0.1% HCOOH, eluent B). Eluent B was increased linearly to 100% in 5 min, kept there 2 min, then back to initial condition in 0.5 min with 2.5-min post run before next injection. Additionally, the sample was eluted with Acquity UPLC® BEH C18 column (100 × 2.1 mm, 1.7 µm Waters Corp., MA, USA) as previously but eluent B was increased linearly to 70% in 10 min, then to 100% in 0.10 min, kept there 3.99 min, and changed back to initial condition in 0.5 min with 5.5-min post run. QTOF was used in resolution mode with positive electrospray ionization. Leucine enkephalin was used as a lock mass, sodium formate and Ultramark® 1621 for mass calibration. Retention times of monosaccharide thiocarbamoyl-thiazolidine derivatives were: D-Man 3.52 min (D-Man 3.52, L-Man 4.22 min), D-Ara 4.41 min (D-Ara 4.89, L-Ara 4.91 min), D-GlcNAc 3.48 min (T_R of D-GlcNAc slightly preceding D-Man T_R according to Tanaka et al. [22] or with C18 column D-GLCNAc 3.95 min (D-GlcNAc 3.94 min, L-GlcNAc not available).

2.4. Description of cell lines and general maintenance

MOLM-13 acute myeloid leukemia cells [23] were cultured in RPMI-1640 medium (R5886, Sigma Life Science, UK) supplemented with 10% (v/v) fetal calf serum (FCS, F7524 Sigma Life Science, UK), 8 mM L-glutamine (Sigma Life Science, UK), and penicillin-streptomycin (100 U ml^{-1} and 0.1 mg ml^{-1} respectively, Sigma Life Science, UK). Normal rat kidney epithelial cells (NRK, ATCC CRL-6509) were cultured in Dulbecco's Eagle's medium (DMEM, D6429, Sigma Life Science, UK) with 10% FCS and penicillin-streptomycin solution. The cells were maintained at 37 °C in 6% CO_2. The cell lines were tested for mycoplasma infection using MycoAlert™ (Lonza Rockland, Inc., USA) every second month. No positive tests were obtained in any cell line during the time of the experiments. *Candida albicans* was obtained as a frozen culture (Department of Clinical Science, University of Bergen, Norway) and grown on solid Sabouraud agar medium at 35 °C. A counting

chamber and appropriate medium or sterile PBS (Sigma-Aldrich, St. Louis, USA) were used to determine cell concentrations when preparing working solutions.

2.5. Cytotoxicity assays

Hassallidin experiments were performed in 96-well culture plates using 300,000 cells ml^{-1} (MOLM-13) or 70,000 cells ml^{-1} (NRK). NRK cells were seeded in the wells the day before the experiments, whereas MOLM-13 suspensions were prepared and seeded in the wells the day of the experiments. Hassallidin D dilutions (prepared in PBS from the 5-mM DMSO stock solutions) were added to the wells containing cells and incubated for 24 h at 37 °C in 6% CO_2. Assessment of cell death was performed using the WST-1 proliferation assay (Roche, Mannheim, Germany) following the manufacturer's instructions, and additionally *via* microscopic evaluation of nuclear and surface morphology of the cells after fixation in 2% buffered formaldehyde containing 0.01 mg ml^{-1} of the DNA-specific fluorescent dye Hoechst 33342 (Sigma-Aldrich, St. Louis, USA). EC_{50} values were estimated by non-linear regression using the statistical software IBM SPSS statistics for Apple (ver. 24, IBM Corp. Armonk, NY, USA):

$$Y = min + \frac{(max - min)}{1 + \left(\frac{IC50}{X}\right)^{h}} \quad (1)$$

where Y is the response (cell death), max and min, the maximum and minimum cell death from the curve, X the concentration of the drug/compound, and h is the hill index. This equation assumes that the EC_{50} point is equal to the inflection point, and that the concave and convex part of the curve has equal geometry. This equation has proved to be a reliable model for curve fitting for cell death induction by various toxins [24,25].

2.6. Transmission electron microscopy of MOLM-13 cells

MOLM-13 cells treated with hassallidin D (**2**) or solvent (for 5, 10, or 15 min with 5, 7.5, or 10 μM concentrations) were fixed with 1.5% glutaraldehyde in 0.1 M sodium cacodylate buffer. After a 2-h fixation at 4 °C, the samples were washed with sodium cacodylate buffer three times. Samples were post-fixed for 1 h with 1% osmium tetroxide in 0.1 M sodium cacodylate buffer and washed twice with sodium cacodylate buffer. Dehydration was prepared with increasing concentrations of ethanol (30–100%) and finally propylene oxide (100%). Samples were infiltrated and embedded into Agar-100 resin and hardened by heating overnight at 60 °C. Ultrathin sections were prepared and imaged with a Jeol JEM-1230 transmission electron microscope at the Molecular Imaging Center, Department of Biomedicine, University of Bergen.

2.7. Flow cytometry

Flow cytometric analyses with propidium iodide (PI, Biolegend, San Diego, USA) were performed with MOLM-13 (460,000 cells ml^{-1}) or *C. albicans* cells (500,000 cells ml^{-1} in PBS from overnight grown plate). Samples treated with hassallidin D (**2**), digitonin (Merck, Darmstadt, Germany) or solvents for 10 min at 37 °C were transferred into Eppendorf tubes and centrifuged at 100 ×*g* for 5 min. After removing 250 μl of supernatant from samples, pellets were dissolved in 200 μl of PBS. PI (0.2 μg ml^{-1}) was added into each sample 5 min before measurement. Samples were measured with an Accuri®C6 flow cytometer using 585/40 (FL2) bandpass filter. Flow cytometry was performed at the Flow Cytometry Core Facility, Department of Clinical Science, University of Bergen. Results were analyzed with FlowJo X program (FlowJo LLC., version 10.3.0). EC_{50} values were estimated by non-linear regression (see Eq. (1) in Section 2.5).

To assess cells for mitochondrial activity, MOLM-13 cells (500,000 cells ml^{-1}) treated with hassallidin D (**2**) or digitonin were incubated for 10 min at 37 °C in 6% CO_2 and centrifuged at 160 ×*g* for 3 min. The supernatants were removed and resuspended in 500 μl of serum-free RPMI medium. After another centrifugation, 250 μl of medium was replaced with an equal volume of 800 nM Mitotracker®Red CM-H_2XRos (M7513, Invitrogen™, Molecular Probes, Inc., Eugene, OR, USA) in serum-free RPMI resulting in a final concentration of 400 nM. The samples were incubated for 45 min at 37 °C in 6% CO_2, washed with 900 μl of pre-warmed PBS, centrifuged at 163 ×*g* for 3 min, and resuspended again in 450 μl PBS. SYTOX™ Blue (S34857, Invitrogen™, Molecular Probes, Inc., Eugene, OR, USA) was added to a final concentration of 0.8 μM 5 min prior to flow cytometric analyses. Samples were analyzed with a BD LSRFortessa™ flow cytometer with bandpass filters 450/50 (407 violet) and 610/20 (561 yellow green) at the Flow Cytometry Core Facility, Department of Clinical Science, University of Bergen. Results were analyzed with FlowJo X program (FlowJo LLC., version 10.3.0).

2.8. Liposome preparations and assays

Liposomes were prepared by creating a phosphatidylcholine (PC) lipid layer from 2.4 mg ml^{-1} Emulmetik™ 930 (Lucas Meyer Cosmetics, France) with or without 0.64 mg ml^{-1} cholesterol (Sigma, St. Louis, USA) in $CHCl_3$ by evaporation in a rotary evaporator. Calcein (Sigma, St. Louis, USA) solution was prepared in a final concentration of 100 mM KCl and 10 mM Tris buffered with NaOH. The pH of the calcein solution was between 6.5 and 7.5. The lipid films were hydrated in the calcein solution at 70 °C and vortexed to create multi-lamellar vesicles (MLV). Liposomes (large unilamellar vesicles) were created by extruding the MLV solution through 0.4-μm and 0.2-μm filters (filter and filter supports were Whatman® Nuclepore™ Track-Etched Membranes, 19 mm, GE Healthcare, UK) using a syringe extruder (Avanti polar lipids, Alabaster, USA) at 65 to 70 °C. Extruded liposomes were then passed through a Sephadex® size-exclusion column (G-50 medium, GE Healthcare, UK) twice with KCl-Tris buffer (pH 7.0) to remove nonencapsulated calcein. The liposome sizes were measured by dynamic light scattering (Malvern Zetasizer Nanoseries, Malvern, UK) and they were on range of 164 to 182 nm.

To find potential role of ergosterol on hassallidin membrane disruption, PC liposomes were produced using 2.4 mg ml^{-1} L-a-phosphatidylcholine (Avanti Polar Lipids, Inc., Alabaster, USA) with or without 0.5 mg ml^{-1} ergosterol (Sigma-Aldrich, St. Louis, USA) in $CHCl_3$. A 43 mM calcein solution (in 10% HEPES buffer with NaOH, pH adjusted to 7.4) was used to rehydrate dried lipid films by heating 70 °C and vortexing. As before, formed MLV's were extruded, and filtered then through size-exclusion column with 10 mM HEPES, 150 mM NaCl solution (pH 7.4). Liposome size measurements were carried out as described above.

To study if changes in liposome concentrations had effects on membrane permeabilization ability of hassallidin, a set of PC liposomes with cholesterol (2.4 mg ml^{-1} L-a-phosphatidylcholine (95%, Avanti Polar Lipids, Inc., Alabaster, USA; 0.65 mg ml^{-1} cholesterol, Sigma, St. Louis, USA)) were prepared. These were prepared with the same calcein and buffer solutions as the ergosterol liposomes.

The release of calcein from liposomes was continuously measured with a fluorescence spectrophotometer (Varian Cary Eclipse, excitation 495, emission 515, Agilent, USA) as described previously [26]. Liposomes were diluted in KCl-Tris (100 mM KCl, 10 mM Tris) or HEPES-NaCl buffer (10 mM HEPES, 150 mM NaCl, pH 7.4) to a total volume of 1 ml. After 30 s recording to confirm stable liposomes, hassallidin D (**2**) or solvent was added. At 11 min, 10% Triton-X was added to release all remaining calcein.

2.9. In silico modeling of hassallidin-membrane interaction

Bilayers were constructed using the CHARMM membrane builder

GUI [27] and converted to Lipid14 PDB format using the charmmlipid2amber.x script [28]. The following two bilayers were constructed: one system containing 128 POPC molecules and another system containing 84 POPC and 44 cholesterol molecules, resulting in a molar percentage of 35 for cholesterol in the second system. Both systems used the TIP3P water model [29] and had 0.15 M KCl salt concentration added to the water layer. Hassallidin was included with identical starting coordinates for both systems. All molecular dynamics simulations were performed with the AMBER 16 software [30] using the GPU-accelerated PMEMD implementation [31]. The full systems were energy minimized and then heated from 0 to 100 K using Langevin dynamics for 5 ps at constant volume with weak restraints on the lipid (force constant of 10 kcal/mol/Å^2). The volume was allowed to adjust as the temperature increased to 300 K, keeping the weak restraint on the lipids. Production runs were then performed at constant pressure (1 atm) regulated by the anisotropic Berendsen method [32] and temperature (300 K) controlled by the Langevin thermostat [33]. Periodic boundary conditions were applied where bonds involving hydrogen were constrained, allowing a 2-fs time step. Structural data was recorded every 10 ps for 300 ns.

3. Results

3.1. Isolation and identification of four hassallidin D variants from cyanobacterium Anabaena sp. UHCC 0258

The cyanobacterium *Anabaena* sp. UHCC 0258 produces different variants of hassallidin C and D [13] from which we aimed to purify hassallidin D with aglyconic core of *m/z* 1283. Four variants of this hassallidin D were purified that differed in their amount of acetyl groups (1–3 acetyl groups in different positions thus yielding variants **1–4**, Fig. 1). Hassallidin D (**2**) with two acetyl groups was the main variant produced by this strain (see UV 280 nm trace in Supplementary Fig. S1A). Hassallidin variants (**1–4**) were identified with HPLC-ITMS and UPLC-QTOF. The behavior of the hassallidin D variants (**1–4**) in HPLC-ITMS (Supplementary Fig. S1) was as reported before [13]. Comparison of the UPLC-QTOF ion mass differences of the four variants to theoretical values resulted in −0.4 to 0 ppm verifying the elemental composition of variants (Supplementary Fig. S1B). The structure of the main hassallidin variant (**2**) was verified with MS and NMR (^{1}H, ^{1}H-^{1}H COSY, ^{1}H-^{1}H TOCSY, ^{1}H-^{13}C HSQC and ^{1}H-^{13}C HMBC, Supplementary Fig. S2). In addition, the identity of monosaccharides, amino acid-monosaccharide connections and locations of the mannose acetyl groups were solved with MS and NMR (Supplementary Figs. S2–S5). The two acetyl groups were situated in positions 4 and 6 in the mannose unit (Supplementary Fig. S6). The annotated ^{1}H-^{13}C HMBC spectrum of the carbonyl region illustrates the connections between amino acids and between acetylated mannoses and acetyl groups (Supplementary Figs. S6 and S7). Altogether, the data demonstrated that the main hassallidin D (**2**) structure was 4,6-diacetylmannose-hassallidin D and that this sample consisted of less than 1% remnants of other variants (Supplementary Fig. S1C). The numerical NMR data (Supplementary Table S1) are consistent with previously published hassallidin NMR data [11–13].

3.2. Hassallidin D variants (1–4) induce cell death in both malignant and normal mammalian cells

Many cyanobacterial compounds show promise as anti-cancer agents [34–36]. We wanted to determine if hassallidins also possessed such activity. However, all four purified hassallidin D variants (**1–4**) were cytotoxic to both acute myeloid leukemia cells (MOLM-13) and normal rat kidney cells (NRK) after 24-h incubation and with no selectivity towards either of the cell types (Fig. 2A–D). In addition, freshly isolated mouse hepatocytes were rapidly affected when treated with hassallidin for 2 h (data not shown). The main variant, hassallidin D (**2**), was the most potent with a half-maximal effective concentration (EC_{50}) of approximately 2.6 µM (Fig. 2B). The other three variants of hassallidin (**1**, **3** and **4**) had EC_{50} values between 3.5 and 5 µM (Fig. 2A, C and D). It should be noted that the EC_{50} values of hassallidin **3** and **4**

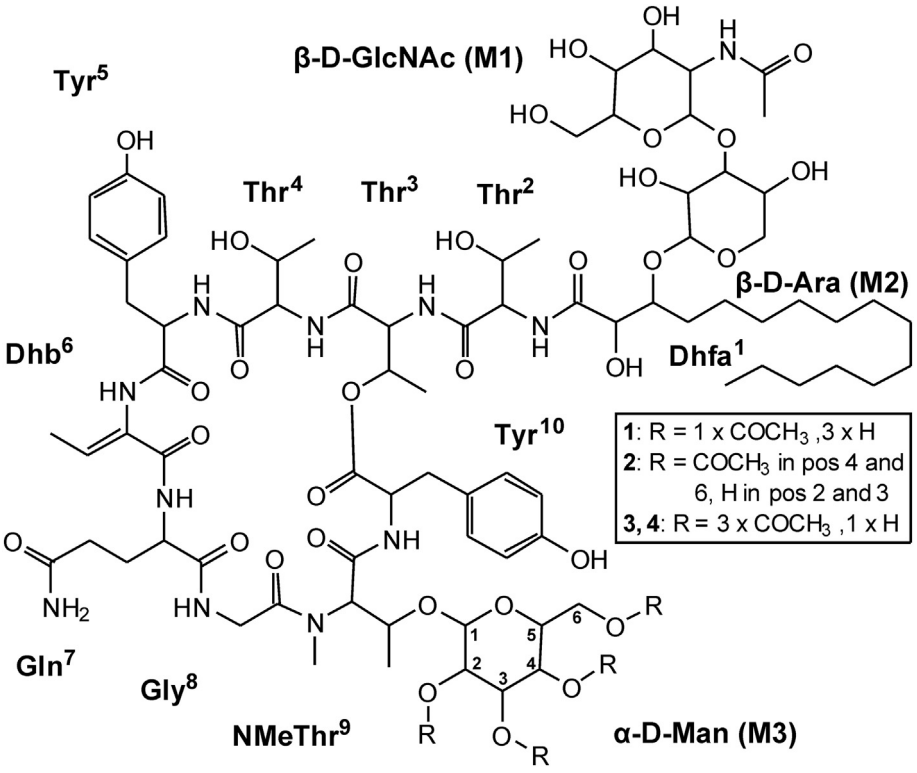

Fig. 1. Chemical structures of four hassallidin D variants (1–4) purified from cyanobacterium *Anabaena* sp. UHCC 0258.

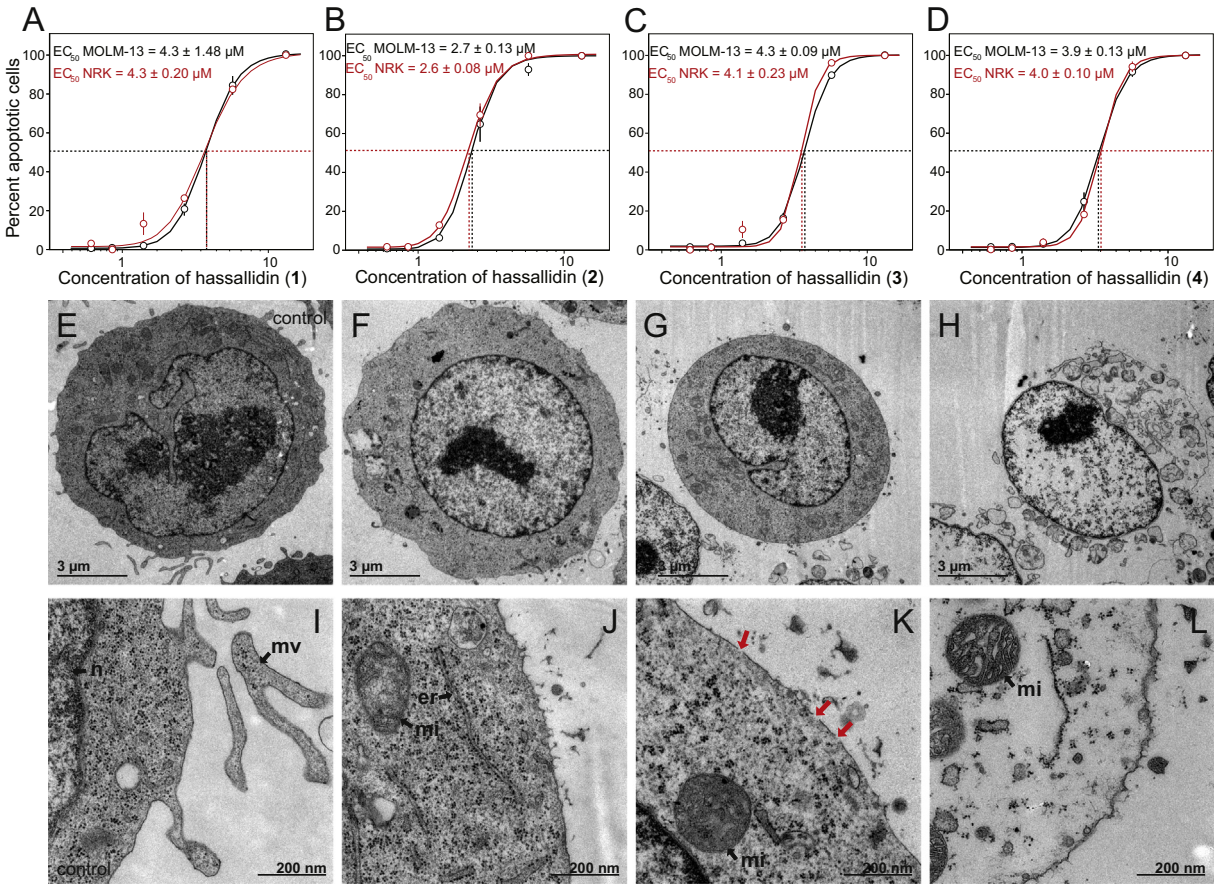

Fig. 2. Hassallidin D induces rapid ruptures in mammalian cell membranes leading to cell death. (A–D) Four hassallidin D variants (**1–4**) exhibit similar effects against two different mammalian cell lines, MOLM-13 and NRK. Results were obtained after a 24-h incubation by fluorescent microscopy counting. Data are shown as means ± SEM (MOLM-13 cells, $n = 6$) or mean ± high and low measurement (NRK, $n = 2$). (E–L) Ultrastructural morphological changes of MOLM-13 cells treated with hassallidin or solvent. The images were chosen to show the different stages of hassallidin-induced cell death from initial membrane effect (F and J) to complete lysis (H and L). The treatments were: E and I: control, F and J: 5 µM for 15 min, G and H: 10 µM 10 min, K: 5 µM 15 min, L: 7.5 µM 5 min. Panels E–H show overviews of single cells and I–L show additional details of the cell organelles and the cell surface membrane. Black arrows in panels indicate the following organelles: mv, microvilli; n, nucleus; er, endoplasmic reticulum; mi, mitochondria, and red arrows show broken or discontinuous cell surface membrane. (For interpretation of the references to color in this figure legend, the reader is referred to the web version of this article.)

have a considerable degree of uncertainty due to the lack of data points inducing cell death between 20 and 90% (Fig. 2C and D). Due to the low yield of the other variants (**1**, **3** and **4**) and the similar behavior in cell assays, further tests were performed using only the main variant, hassallidin D (**2**). Additionally, the incubation time was reduced in further tests, as the effects of hassallidins were observed after less than one hour (data not shown).

3.3. Ultrastructural analysis reveals membrane disruption caused by hassallidin D

To study more specifically how hassallidin affects eukaryotic cells, we prepared transmission electron microscopy (TEM) slides from MOLM-13 cells treated with hassallidin for 5 to 15 min (Fig. 2E–L). The first signs of morphological changes were disappearance of microvilli and smoothing of the cellular surface (Fig. 2F and J). At the same time, the cytoplasm became less dense and the nucleus changed shape to become more rounded with a smooth appearance. We next observed that the cell surface membrane was broken or discontinuous with gaps of several micrometers in length (Fig. 2K). Finally, the cell membrane was completely disintegrated and the cytoplasm disappeared, leaving only organelles and the nucleus (Fig. 2H and L). However, the mitochondria were easily distinguishable throughout the cell death process (Fig. 2J, K, L) and appeared unharmed even when the remainder of the cell had disintegrated (Fig. 2L).

3.4. Hassallidin D induces rapid lysis of eukaryotic cell membrane allowing internalization of small molecules

The cytotoxic effects of hassallidin on cell viability were confirmed with propidium iodide (PI) staining of MOLM-13 cells. This method detects loss of cell surface membrane integrity by measuring increased PI internalization [37]. Increasing hassallidin concentrations resulted in a higher number of PI-positive cells (Fig. 3), which is consistent with the ultrastructural findings (Fig. 2E–L). There was a marked increase in PI internalization at 2.5 µM hassallidin and almost all cells were PI positive at 5 µM (Fig. 3A). The EC_{50} for hassallidin-induced PI internalization was 4.8 µM after a 15-min incubation (Fig. 3B). We compared the effect with that of the biodetergent digitonin [26,38,39]. While both digitonin and hassallidin seemed to affect the cells similarly, digitonin was slightly less potent with an EC_{50} of 6.5 µM (Fig. 3B). Since hassallidin has shown antifungal activities [11–14,16], we examined if membrane disruption also occurred in *Candida albicans* treated with hassallidin and compared again with digitonin (Fig. 3C and D). A significantly higher concentration of hassallidin or digitonin was required to cause PI internalization into yeast cells after a 15-min incubation (Fig. 3C and D). The EC_{50} for *C. albicans* was approximately 30 µM for both hassallidin and digitonin (Fig. 3D).

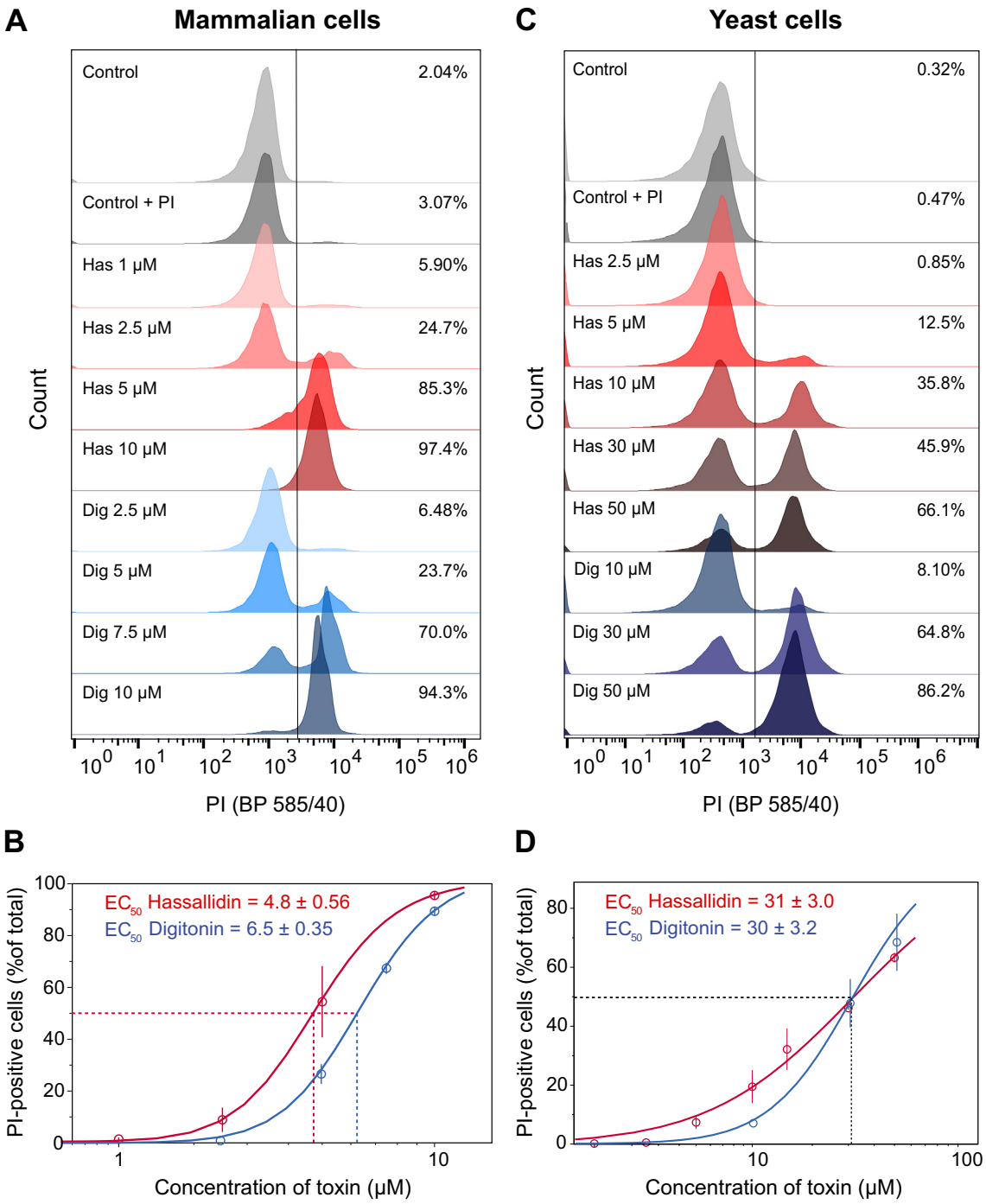

Fig. 3. Hassallidin D or digitonin treatment induces propidium iodide (PI) internalization into eukaryotic cells due to membrane permeabilization. (A) Internalization of propidium iodide (PI) in human (MOLM-13) cells treated with hassallidin or digitonin represented as histograms. (B) Dose-response curve of PI internalization into MOLM-13 cells treated with hassallidin or digitonin with calculated EC_{50} values. (C) Internalization of PI in yeast (*Candida albicans*) cells treated with hassallidin or digitonin. (D) Dose-response curve of PI internalization into *C. albicans* yeast cells treated with hassallidin or digitonin with calculated EC_{50} values. Note the different concentrations of compounds used in mammalian or yeast cells. Vertical lines in histograms represent PI gating (see Supplementary Fig. S8 for gating strategy). Percentages of nonviable or dead cells are shown in the histograms for each sample. The data in B and D are average ± SEM of four (B) or five (D) parallel experiments. The EC_{50} values were calculated by four-parameter regression analyses in SPSS (see Materials and methods Section 2.5 for details).

3.5. Hassallidin D distinguishes between mitochondrial and cell surface membranes

Although hassallidin D caused membrane disruption inevitably leading to cell death, TEM images indicated that not all cellular constituents were affected equally (Fig. 2H and L). To determine if the mitochondria were functional after membrane disintegration, we double-stained MOLM-13 cells with SYTOX™ Blue for membrane integrity and Mitotracker®Red CM-H_2XRos to detect viable mitochondria (see Supplementary Fig. S9 for details on gating strategy). Similar to PI (Fig. 3), we observed an increase in SYTOX™ Blue-positive cells with increasing hassallidin or digitonin concentrations (Fig. 4). However, the decline in mitochondrial function did not follow the decline in cell surface membrane integrity (Fig. 4D and H). Functional mitochondria

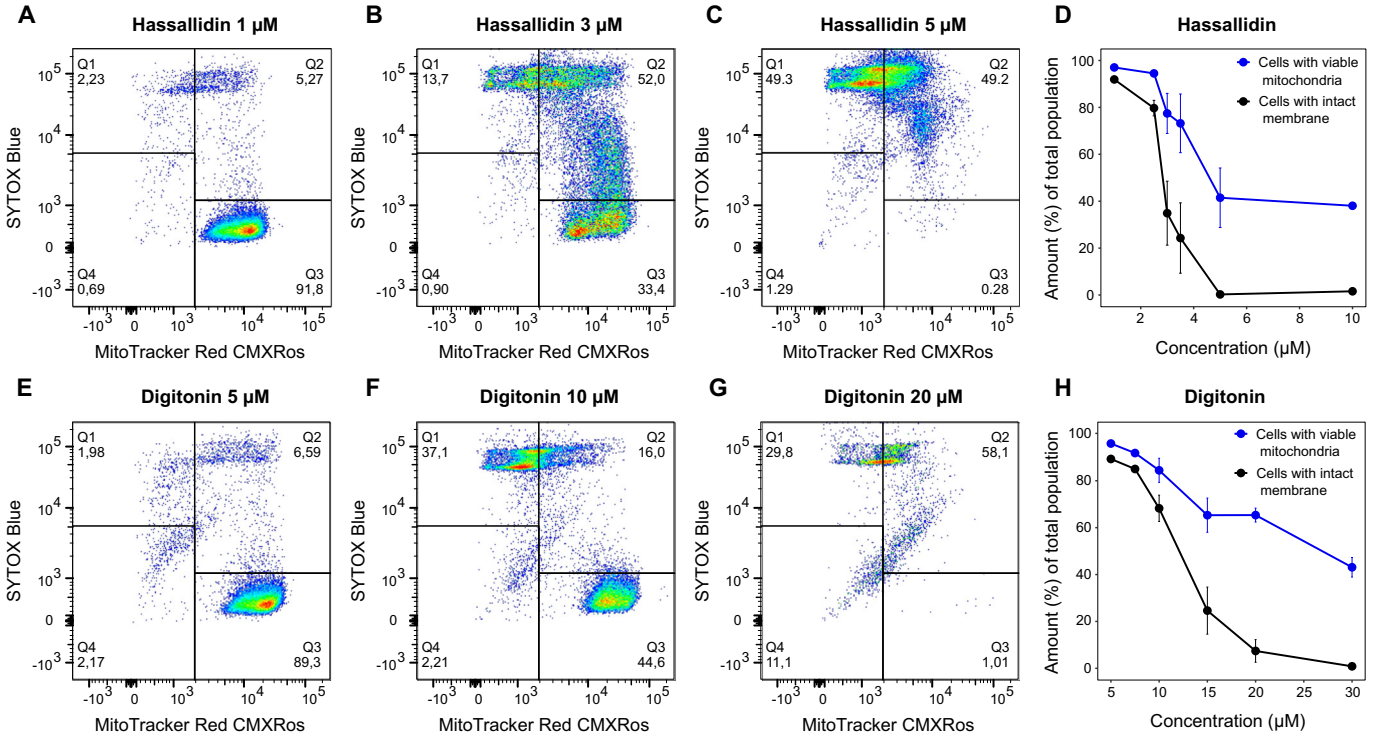

Fig. 4. Mitochondria remain viable and functional after hassallidin-induced lysis of cell surface membrane. (A–C) Scatter plots showing Mitotracker®Red CM-H2XRos (X-axis) and SYTOX™ Blue (Y-axis) staining of human MOLM-13 cells after treatment of different concentrations of hassallidin for approximately 15 min. (D) Dose-response curve of MOLM-13 cells treated with increasing concentrations of hassallidin showing cells with viable mitochondria and cells with intact cell membrane. (E–G) As in A to C but with different concentrations of digitonin. (H) As in D but with digitonin. The data in D and H are average ± SEM from 3 to 5 parallel experiments, except the last concentrations (10 or 30 μM) represent only one or two parallels. The gating strategy for the flow analyses is shown in Supplementary Fig. S9. Q1, SYTOX™ Blue; Q2, SYTOX™ Blue and Mitotracker®Red CM-H2XRos; Q3, Mitotracker®Red CM-H2XRos; Q4, no staining. (For interpretation of the references to color in this figure legend, the reader is referred to the web version of this article.)

were observed even at 5 μM hassallidin, a concentration at which almost all cells were broken or dead (Fig. 4C). The observed difference between mitochondria and cell surface membrane disruption was similar for both hassallidin (Fig. 4A–C) and digitonin (Fig. 4E–G).

3.6. Hassallidin D shows cholesterol-dependent membrane disruption on artificial membranes and in silico

One of the main differences between mitochondrial and cell surface membranes is cholesterol content. Mitochondria have significantly lower amounts of sterols in their membranes [40]. To determine if the presence of cholesterol was the limiting factor for hassallidin activity, we studied the effects of hassallidin on cell membranes by constructing liposomes with membranes of pure phospholipids or of phospholipids and cholesterol. Addition of hassallidin into the suspension of cholesterol-containing liposomes caused an immediate release of calcein from the liposomes, which was seen as a rapid increase of fluorescence intensity (Fig. 5A). At 0.8 μM concentration, hassallidin caused almost complete release of calcein from the liposomes within 1 min. A reduction to 0.4 μM hassallidin caused significant calcein release, which did not stabilize during the time of the experiment (11 min), indicating that the liposomal membrane was permanently disrupted. We did not detect any calcein release from the liposomes at 0.3 μM hassallidin, suggesting that the membrane was intact. In contrast, the liposomes without cholesterol in their membrane exhibited only modest calcein release even after treatment with 30 μM hassallidin (Fig. 5B), corresponding to the amount observed with 0.4 μM hassallidin in the cholesterol-containing liposomes (Fig. 5A). Moreover, we observed an initial leakage, which stopped since the curve appeared to flatten (Fig. 5B, black line). Hassallidin thus showed specific membrane-disrupting activity against cholesterol-containing membranes (Fig. 5). The fungal membranes contain ergosterol instead of cholesterol. To reveal if either of these sterols were necessary for hassallidin-induced permeabilization, we produced liposomes with ergosterol instead of cholesterol. Ergosterol liposomes were also highly sensitive to hassallidin (Fig. 5C). The apparent decrease in signal over time seen in Fig. 5C and D could be attributed to fading of the fluorophore by the UV spectrophotometer, or by quenching of the released calcein. The hassallidin concentration required for the disruption of ergosterol liposomes was slightly higher than for cholesterol liposomes, which could be attributed to a different batch of PC from a different supplier (see the Materials and methods Section 2.8 for details). By repeating leakage assay with different concentrations of cholesterol liposomes, a logical trend was observed that more hassallidin is needed to produce the same effect in higher amount of liposomes (Supplementary Fig. S10).

We further studied the effects of hassallidin on lipid membranes by *in silico* simulations of hassallidin in complex with 1-palmitoyl-2-oleoyl-sn-glycero-3-phosphatidylcholine (POPC) bilayers with or without embedded cholesterol (Fig. 6, Supplementary Videos S1 and S2). The *in silico* modeling supported the finding of cholesterol dependency (Fig. 5A) in that hassallidin acyl chain inserted into the bilayer when cholesterol was present (Fig. 6A, C, E). Hassallidin only slightly interacted with the surface of the phosphatidylcholine bilayer (without insertion) when cholesterol was not present (Fig. 6B, D, F). There was rapid insertion of the fatty acid into the membrane with cholesterol (Fig. 6C) accompanied by association of the tyrosine-5 ring into the polar part of the lipid membrane (Fig. 6E). Calculated order parameters together with visual inspection of the bilayer trajectories showed that cholesterol induces an ordering of the POPC fatty acids together with a straightening of the aliphatic chains (Fig. 6G and H). Cholesterol thus increases the distance between phosphate groups of each leaflet in the bilayer from slightly below to slightly above 40 Å (Fig. 6C-F, red

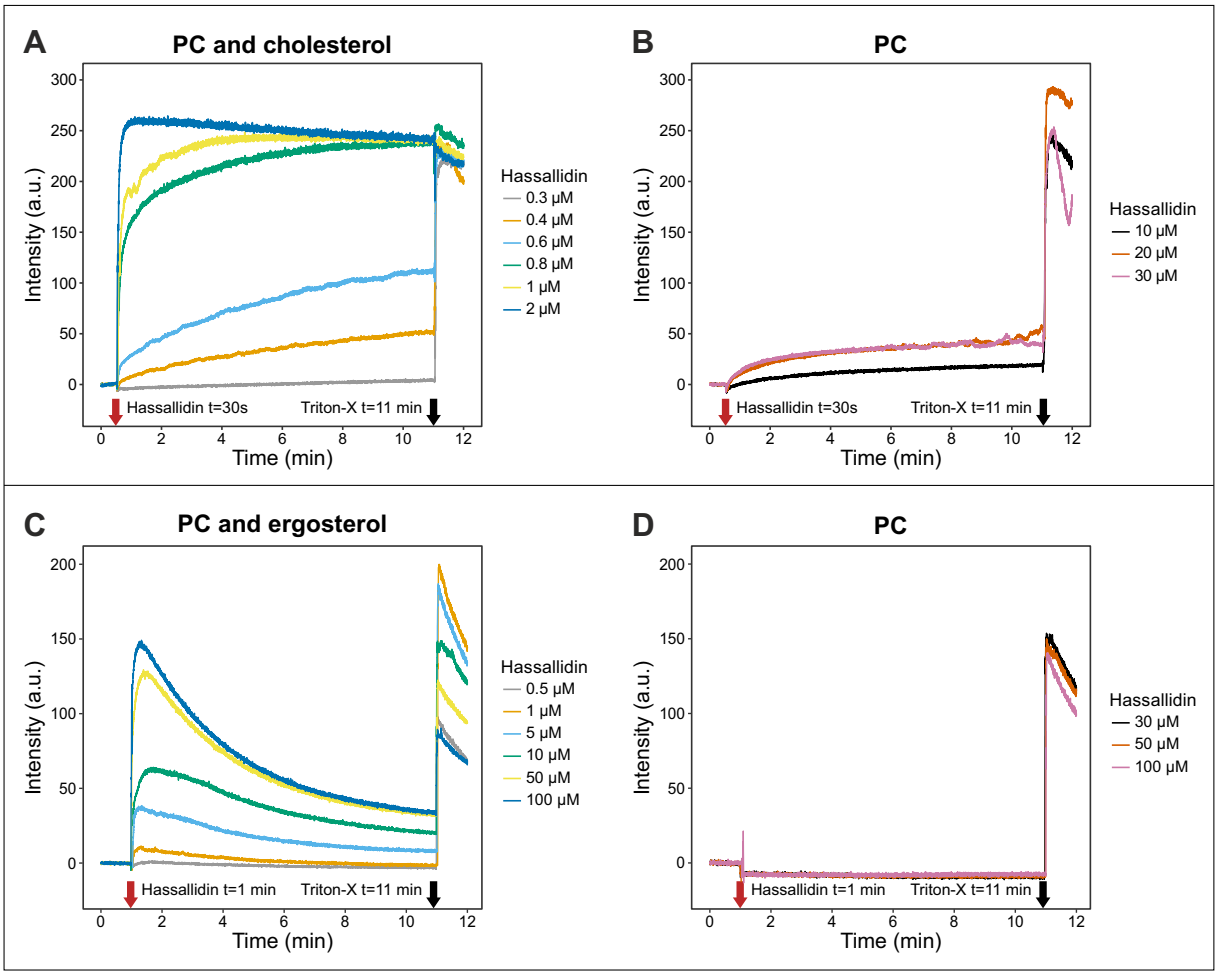

Fig. 5. Hassallidin D exhibit sterol-dependent activity. (A) Disruption of liposomes prepared from phosphatidylcholine (PC) and cholesterol, visualized by the release of the fluorescent compound calcein (fluorescence intensity measured). (B) Disruption of liposomes prepared from PC only. Note the different concentrations used in A and B. The red arrows indicate the addition of hassallidin and the black arrows indicate addition of detergent Triton-X to induce maximal calcein release. (C) Disruption of liposomes made from PC and ergosterol and (D) PC liposomes only. The PC used in C and D was of a different quality compared to that in A and B, which explains the discrepancy in the calcein release between B and D. Note also the (unidentified) quenching of fluorescence in C and D. Hassallidin has remained stable in the sample during the storage (QTOF verification), thus results are comparable (A and C) regardless of unknown quenching. (For interpretation of the references to color in this figure legend, the reader is referred to the web version of this article.)

traces).

4. Discussion

The cyclic glycolipopeptide hassallidins are mostly known from their antifungal activities and their wide distribution among cyanobacteria [11–14,16]. However, their mechanism of action has remained unclear. In this study, purified hassallidin D variants from cyanobacterium *Anabaena* sp. UHCC 0258 were shown to have general toxicity on mammalian cells, including normal and malignant cells. Furthermore, hassallidin D (**2**) induced permeabilization of the surface membrane but left mitochondria viable. Experiments on isolated membrane systems revealed that hassallidin D (**2**) preferentially disrupts sterol-containing membranes.

The four purified hassallidin D variants (**1–4**) showed cytotoxic effects against eukaryotic cells (Fig. 2). Ultrastructural analysis (Fig. 2C–L) together with PI internalization (Fig. 3) demonstrated that hassallidin D (**2**) rapidly disrupted cell membranes. The lack of mitochondrial lysis (Fig. 2J–L), and the fact that mitochondria were functional after surface membrane disruption (Fig. 4) is in line with their low sterol content, reported to be about 10 times lower than in eukaryotic surface membranes [40,41]. Among the many cytotoxic compounds described from cyanobacteria, there are only few compounds that have shown similar membrane lytic effects. Anabaenolysins isolated from *Anabaena* sp. and muscotoxins from *Desmonostoc muscorum* have shown similar results in cellular and liposomal assays [8,26]. However, muscotoxins permeabilize liposomes without cholesterol [8]. Thus, the effects of anabaenolysin and hassallidin seem to be analogous and even the EC_{50} values for cytotoxicity of hassallidin and anabaenolysin are similar [26].

Similar to the anabaenolysins, our results indicated that the effects of hassallidin may resemble surface-active compounds such as the saponin digitonin. Digitonin is known to specifically interact with cholesterol in membranes, which then causes changes in cell surface membrane curvature [38,39]. Hassallidin D (**2**) was also dependent on cholesterol as it specifically disrupted artificial liposomes prepared with cholesterol and phosphatidylcholine (Fig. 5). These observations are similar to those of digitonin in liposomal assay [26]. In addition to digitonin and anabaenolysin, there are other natural products that permeabilize membranes and associate with sterols, such as theonellamide A [42] and iturins [43–45].

While hassallidins are structurally different from the other membrane-active molecules mentioned above, it shares the presence of a fatty acid moiety. *In silico* modeling revealed that the first contact

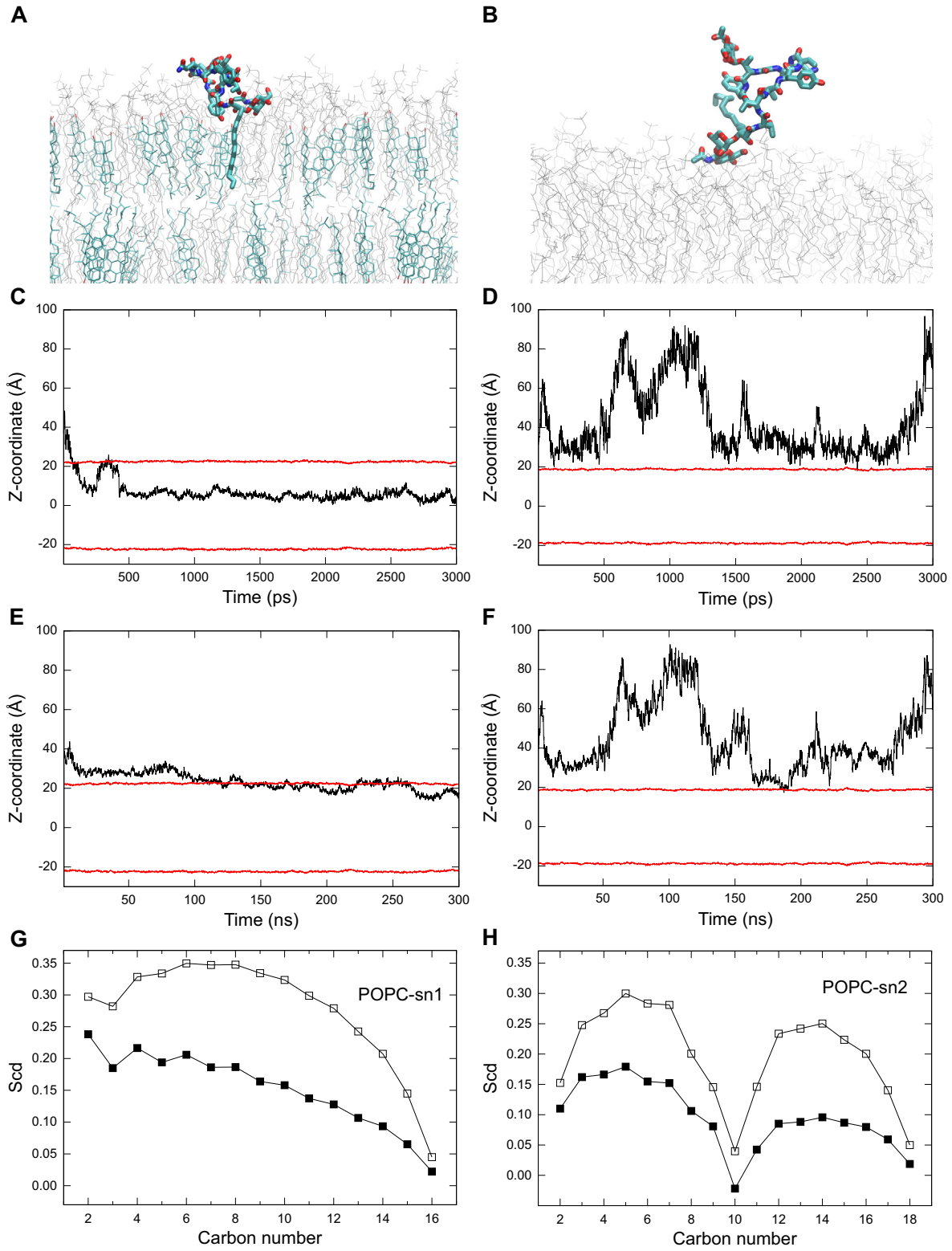

Fig. 6. Hassallidin D inserts into membranes with cholesterol in an *in silico* model. (A–B) Snapshots of hassallidin at 150 ns simulation time in the presence of POPC/cholesterol (A) and POPC bilayers (B). (C–D) Panels show the average *Z*-coordinate (corresponding to the bilayer normal) of phosphate groups in each bilayer leaflet (red lines) together with the Z-coordinate of the terminal CH_3-group in the hassallidin aliphatic tail, as a function of simulation time for the membranes with (C) and without cholesterol (D). (E–F) Panels show the Z-coordinate of the tyrosine-5 ring in hassallidin (center of mass) as a function of simulation time for the membranes with (E) and without (F) cholesterol. The red lines again correspond to the average Z-coordinate of the phosphate atoms of each leaflet in both panels. In panels C to F, the Z-coordinate of zero corresponds to the center of the bilayer. (G–H) The final two panels show the calculated deuterium order parameters (S_{cd}) of the sn-1 (Panel G) and sn-2 fatty acids (Panel H) in POPC for the simulation with (open squares) and without (black squares) cholesterol. (For interpretation of the references to color in this figure legend, the reader is referred to the web version of this article.)

between hassallidin and the membrane was through the amino acids of the hassallidin, and the lipid tail of hassallidin inserted into the cholesterol-containing membrane immediately after (Fig. 6A and Supplementary Video S1). Interestingly, hassallidin seemed to enter deeper into the membrane during the course of the *in silico* modeling (Fig. 6C and E and Supplementary Video S1). The conformation of hassallidin remained quite stable during invasion into the cholesterol-containing membrane when compared with membranes without cholesterol. The lipid tail insertion into the membrane alone is not expected to break the membrane. However, the large polar head of the hassallidin molecule generates a very conical geometry. When the hassallidin has inserted into the membrane, it may change the membrane curvature to become more convex, and the membrane structure is eventually disrupted, as has been described for surfactin [46]. If this was the case, one could expect that there must be a minimal ratio of hassallidin molecules per area of lipid membrane. This can be found by investigating whether the concentration of lipids influences the efficacy of hassallidin (*e.g.* the concentration needed to obtain 50% release of calcein). We found that higher lipid concentrations needed higher hassallidin concentration to obtain the same effect (Supplementary Fig. S10), showing that hassallidin-induced membrane disruption is not a local effect, but rather dependent on a certain partitioning between hassallidin and lipids [47].

In our model of one hassallidin molecule, hassallidin did not seem to interact directly with cholesterol such as observed for digitonin [38,39], suggesting that cholesterol may simply provide a better organized and structured membrane, which enables hassallidin insertion. The thickening of the bilayer (Fig. 6C–E, red lines) and ordering of the fatty acids observed (Fig. 6G and H) are in agreement with previous studies on membranes with increasing cholesterol content as shown both experimentally and in simulations [48,49]. Although the simulation does not cover the timeframe needed to reach steady state conditions for hassallidin insertion into membrane, it still fits with the data obtained with liposomes (Fig. 5). We would expect some interaction with non-cholesterol membranes at higher hassallidin to lipid ratio and simulation run at longer time-frames, in line with what was observed in Fig. 5B. Also, due to the limited number of molecules, our model is not able to provide an exact molecular explanation for the disruption of the bilayer integrity. To obtain this, a much larger model with several hassallidin molecules must be made on a longer time-scale, which is not possible with our all-atom model. Membrane-permeabilization compounds may have a specific attachment route, such as digitonin with cholesterol [38,39]. Some compounds are known to create a channel through the membrane by creating a complex of several molecules [50], while some compounds may have more than one mode of action. For example, amphotericin B has been found to bind directly to ergosterol in addition to its channel-formation activities [51]. However, the target of hassallidins is clearly the cell surface membrane; this was already hypothesized in the study where the effects of hassallidin A against *C. albicans* were compared to those of the echinocandin antifungal caspofungin due to their structural similarities [18], and confirmed here.

It has been shown that the activity of hassallidin is diminished by the opening of the ring structure [13]. This demonstrates that there are elements in the ring structure that are essential for obtaining a close association with the membrane and to direct the fatty acid moiety towards the inner core of the membrane bilayer (for example, compare Fig. 6A and C with Fig. 6B and D). From *in silico* modeling, we observed that hassallidin associates several times with the membrane without cholesterol, but then dissociates rapidly. After the first contact between hassallidin and the cholesterol-containing membrane, the tyrosine-5 is located close to the membrane, eventually being located inside the outer phosphate atoms of the phospholipids (Fig. 6E). Since the linear variant of hassallidin is less potent [13], the spatial relationship between the fatty acid and the aromatic amino acids appears to be important to induce membrane insertion and eventually lysis.

Hassallidin variants A to E and balticidins are found from a large variety of cyanobacteria [11–15,52], and there are also other prokaryote compounds that structurally belong to the hassallidin family and have similar antifungal activity. Thus, hassallidins and balticidins from cyanobacteria, herbicolins from *Erwinia herbicola* [53], jagaricin from *Janthinobacterium agaricidamnosum* [54], chromobactomycin from *Chromobacterium* sp. C61 [55], and Sch 20561 and Sch 20562 from *Aeromonas* sp. W-10 [56,57] all share a similar glycopeptide structure attached to a lipid tail with varying lengths. These molecules do not possess antibacterial activities with the exception of the antimycobacterial activities of herbicolin A [58]. The sterol dependency of hassallidin D could explain the absence of antibacterial activity, as bacterial membranes generally do not contain sterols (see [59] for a review on sterols in microorganisms). The effects of these molecules against mammalian cells have been reported only for a few cell lines [16]. We directly compared the effects of hassallidin D on human and yeast cells and observed that both hassallidin and digitonin were more potent against human cell lines compared than against *C. albicans* (Fig. 3). This could be explained by the presence of a cell wall in yeast, which makes the surface membrane less accessible to the toxins. Hassallidins are still effective compounds against a range of opportunistic fungi. The EC_{50} for PI internalization into *C. albicans* was approximately 30 μM (Fig. 3D), which is higher than reported MIC values (MIC 1.5–16 μM, IC_{50} 0.3–1 μM) [11–13,16]. The discrepancy between our findings on PI internalization and previous MIC data can be explained by the difference in assay. Whereas PI internalization reports membrane intactness during a few minutes, and is not a measure of viability, MIC gives an indication of the proliferation rate of the culture over longer time period. The latter could be influenced by mechanisms that are not detectable in a membrane intactness assay like ours. In conclusion, hassallidins seem to have general toxicity against eukaryotic cells, which all have sterols in their membranes. Accordingly, hassallidins are unlikely candidates for antifungal drugs.

The ecological rationale for producing hassallidin or related compounds is still unknown. Nevertheless, many different bacterial species produce these compounds and the geographical range of habitats is constantly increasing [13,60]. This suggests that these compounds provide an evolutionary benefit. The ecological interactions of the microbial compounds may be very complicated. It was recently shown that the antifungal effect of anabaenolysin was enhanced by cyclodextrins, which were also produced by the same cyanobacteria [61]. The biodetergent digitonin has also been found to enhance drug effects [62,63]. Further research could be focused on the interactions of hassallidin with other compounds or if hassallidins already have a natural co-effector compound.

5. Conclusions

Microbial natural products participate in complex ecological webs by acting as for instance defense or signal molecules. Many of these products are also valuable to humans as pharmaceuticals or in biotechnological applications. Through the identification and observation of natural products, their ecological role can be understood and their potential for other applications can be evaluated. Here, we studied the antifungal and cytotoxic cyclic glycolipopeptide hassallidin D. We determined the mechanism of action for hassallidin D purified from cyanobacterium *Anabaena* sp. UHCC 0258. We observed that hassallidin D specifically disrupts sterol-containing cell surface membranes. Many cyanobacteria strains have been identified as hassallidin producers from different habitats and other microbes produce hassallidin family compounds as well, which indicates that membrane-effective compounds play an important ecological role.

Supplementary data to this article can be found online at https://doi.org/10.1016/j.bbamem.2019.03.010.

Author contributions

Anu Humisto: Conceptualization, Data curation, Formal analysis,

Investigation, Methodology, Visualization, Writing, original draft, Writing, review and editing.

Jouni Jokela: Data curation, Formal analysis, Investigation, Methodology, Visualization, Writing, original draft.

Knut Teigen: Data curation, Formal analysis, Investigation, Methodology, Visualization, Writing, original draft.

Matti Wahlsten: Data curation, Formal analysis, Investigation.

Perttu Permi: Formal analysis, Investigation.

Kaarina Sivonen: Conceptualization, Funding acquisition, Supervision, Methodology, Writing, review and editing.

Lars Herfindal: Conceptualization, Data curation, Formal analysis, Funding acquisition, Methodology, Visualization, Writing, original draft, Writing, review and editing.

Transparency document

The Transparency document associated with this article can be found, in online version.

Declaration of Competing Interest

The authors declare no competing interests.

Acknowledgements

We sincerely thank Brith Bergum for maintaining the Flow Cytometry Core Facility at University of Bergen for her help in flow cytometric analyses. TEM imaging was performed at the Molecular Imaging Center, Department of Biomedicine, University of Bergen. *C. albicans* was kindly provided by Prof. Audun Helge Nerland (Department of Clinical Science, University of Bergen). Hideo Iwai and Tuomas Niemi-Aro (Institute of Biotechnology, University of Helsinki, Finland) are thanked for the use of 850 MHz NMR instrument (the NMR core facility at the Institute of Biotechnology is funded by Biocenter Finland). Uninett Sigma2 AS is acknowledged for providing infrastructure and computer time for the molecular dynamics simulations.

Funding sources

This work was supported by a Jane and Aatos Erkko Foundation (Finland) grant to K.S., the Academy of Finland grant 288235 to P.P., and the Norwegian Cancer Society and Western Norway Health Authorities to L.H. K.S. and L.H. also received funding from the NordForsk NCoE Programme “NordAqua” (project #82845). A.H. was funded by the Doctoral Programme in Microbiology and Biotechnology (University of Helsinki, Department of Microbiology).

References

[1] A.M. Burja, B. Banaigs, E. Abou-Mansour, J. Grant, P.C. Wright, Marine cyanobacteria — a prolific source of natural products, Tetrahedron. 57 (2001) 9347–9377, https://doi.org/10.1016/S0040-4020(01)00931-0.

[2] R.K. Singh, S.P. Tiwari, A.K. Rai, T.M. Mohapatra, Cyanobacteria: an emerging source for drug discovery, J. Antibiot. (Tokyo) 64 (2011) 401–412, https://doi.org/10.1038/ja.2011.21.

[3] E. Dittmann, M. Gugger, K. Sivonen, D.P. Fewer, Natural product biosynthetic diversity and comparative genomics of the cyanobacteria, Trends Microbiol. 23 (2015) 642–652, https://doi.org/10.1016/j.tim.2015.07.008.

[4] S.S. Moon, J. Lu Chen, R.E. Moore, G.M.L. Patterson, Calophycin, a fungicidal cyclic decapeptide from the terrestrial blue-green alga *Calothrix fusca*, J. Organomet. Chem. 57 (1992) 1097–1103, https://doi.org/10.1021/jo00030a013.

[5] W.P. Frankmölle, G. Knübel, R.E. Moore, G.M. Patterson, Antifungal cyclic peptides from the terrestrial blue-green alga *Anabaena laxa*, J. Antibiot. (Tokyo) 45 (1992) 1458–1466, https://doi.org/10.7164/antibiotics.45.1458.

[6] J.B. MacMillan, M.A. Ernst-Russell, J.S. De Ropp, T.F. Molinski, Lobocyclamides A-C, lipopeptides from a cryptic cyanobacterial mat containing *Lyngbya confervoides*, J. Organomet. Chem. 67 (2002) 8210–8215, https://doi.org/10.1021/jo0261909.

[7] N. Maru, O. Ohno, D. Uemura, Lyngbyacyclamides A and B, novel cytotoxic peptides from marine cyanobacteria *Lyngbya* sp, Tetrahedron Lett. 51 (2010) 6384–6387, https://doi.org/10.1016/j.tetlet.2010.06.105.

[8] P. Tomek, P. Hrouzek, M. Kuzma, J. Sýkora, R. Fišer, J. Černý, P. Novák, S. Bártová, P. Šimek, M. Hof, D. Kavan, J. Kopecký, Cytotoxic lipopeptide muscotoxin A, isolated from soil cyanobacterium *Desmonostoc muscorum*, permeabilizes phospholipid membranes by reducing their fluidity, Chem. Res. Toxicol. 28 (2015) 216–224, https://doi.org/10.1021/tx500382b.

[9] P. Hrouzek, M. Kuzma, J. Černý, P. Novák, R. Fišer, P. Šimek, A. Lukešová, J. Kopecký, The cyanobacterial cyclic lipopeptides puwainaphycins F/G are inducing necrosis via cell membrane permeabilization and subsequent unusual actin relocalization, Chem. Res. Toxicol. 25 (2012) 1203–1211, https://doi.org/10.1021/tx300044t.

[10] J. Jokela, L. Oftedal, L. Herfindal, P. Permi, M. Wahlsten, S.O. Døskeland, K. Sivonen, Anabaenolysins, novel cytolytic lipopeptides from benthic *Anabaena* cyanobacteria, PLoS One 7 (2012) e41222, , https://doi.org/10.1371/journal.pone.0041222.

[11] T. Neuhof, P. Schmieder, K. Preussel, R. Dieckmann, H. Pham, F. Bartl, H. von Döhren, Hassallidin A, a glycosylated lipopeptide with antifungal activity from the cyanobacterium *Hassallia* sp, J. Nat. Prod. 68 (2005) 695–700, https://doi.org/10.1021/np049671r.

[12] T. Neuhof, P. Schmieder, M. Seibold, K. Preussel, H. von Döhren, Hassallidin B -second antifungal member of the Hassallidin family, Bioorg. Med. Chem. Lett. 16 (2006) 4220–4222, https://doi.org/10.1016/j.bmcl.2006.05.094.

[13] J. Vestola, T.K. Shishido, J. Jokela, D.P. Fewer, O. Aitio, P. Permi, M. Wahlsten, H. Wang, L. Rouhiainen, K. Sivonen, Hassallidins, antifungal glycolipopeptides, are widespread among cyanobacteria and are the end-product of a nonribosomal pathway, Proc. Natl. Acad. Sci. U. S. A. 111 (2014) E1909–E1917, https://doi.org/10.1073/pnas.1320913111.

[14] C. Pancrace, J. Jokela, N. Sassoon, C. Ganneau, M. Desnos-Ollivier, M. Wahlsten, A. Humisto, A. Calteau, S. Bay, D.P. Fewer, K. Sivonen, M. Gugger, Rearranged biosynthetic gene cluster and synthesis of hassallidin E in *Planktothrix serta* PCC 8927, ACS Chem. Biol. 12 (2017) 1796–1804, https://doi.org/10.1021/acschembio.7b00093.

[15] T.H. Bui, V. Wray, M. Nimtz, T. Fossen, M. Preisitsch, G. Schröder, K. Wende, S.E. Heiden, S. Mundt, Balticidins A-D, antifungal hassallidin-like lipopeptides from the Baltic Sea cyanobacterium *Anabaena cylindrica* Bio33, J. Nat. Prod. 77 (2014) 1287–1296, https://doi.org/10.1021/np401020a.

[16] T. Neuhof, R. Dieckmann, H. von Döhren, K. Preussel, M. Seibold, P. Schmieder, Lipopeptides having pharmaceutical activity. Patent analysis, EP 1698638 A1, 1–32, 2006.

[17] H. Wang, K. Sivonen, L. Rouhiainen, D.P. Fewer, C. Lyra, A. Rantala-Ylinen, J. Vestola, J. Jokela, K. Rantasärkkä, Z. Li, B. Liu, Genome-derived insights into the biology of the hepatotoxic bloom-forming cyanobacterium *Anabaena* sp. strain 90, BMC Genomics 13 (2012) e613, https://doi.org/10.1186/1471-2164-13-613.

[18] T. Neuhof, M. Seibold, S. Thewes, M. Laue, C.O. Han, B. Hube, H. von Döhren, Comparison of susceptibility and transcription profile of the new antifungal hassallidin A with caspofungin, Biochem. Biophys. Res. Commun. 349 (2006) 740–749, https://doi.org/10.1016/j.bbrc.2006.08.110.

[19] J. Kótai, Instructions for preparation of modified nutrient solution Z8 for algae, Nor. Inst. Water Res. 11 (1972) 1–5 (Oslo, Norway).

[20] J.L. Giner, J. Feng, D.J. Kiemle, NMR tube degradation method for sugar analysis of glycosides, J. Nat. Prod. 79 (2016) 2413–2417, https://doi.org/10.1021/acs.jnatprod.6b00180.

[21] Y.-H. Wang, B. Avula, X. Fu, M. Wang, I.A. Khan, Simultaneous determination of the absolute configuration of twelve monosaccharide enantiomers from natural products in a single injection by a UPLC-UV/MS method, Planta Med. 78 (2012) 834–837.

[22] T. Tanaka, T. Nakashima, T. Ueda, K. Tomii, I. Kouno, Facile discrimination of aldose enantiomers by reversed-phase HPLC, Chem. Pharm. Bull. (Tokyo) 55 (2007) 899–901, https://doi.org/10.1248/cpb.55.899.

[23] Y. Matsuo, R.A.F. MacLeod, C.C. Uphoff, H.G. Drexler, C. Nishizaki, Y. Katayama, G. Kimura, N. Fujii, E. Omoto, M. Harada, K. Orita, Two acute monocytic leukemia (AML-M5a) cell lines (MOLM-13 and MOLM-14) with interclonal phenotypic heterogeneity showing MLL-AF9 fusion resulting from an occult chromosome insertion, ins(11;9)(q23;p22p23), Leukemia. 11 (1997) 1469–1477, https://doi.org/10.1038/sj.leu.2400768.

[24] M. Vu, L. Herfindal, O.J. Juvik, A. Vedeler, S. Haavik, T. Fossen, Toxic aromatic compounds from fruits of *Narthecium ossifragum* L, Phytochemistry. 132 (2016) 76–85, https://doi.org/10.1016/j.phytochem.2016.09.010.

[25] R. Bjørnstad, R. Aesoy, Ø. Bruserud, A.K. Brenner, F. Giraud, T.H. Dowling, G. Gausdal, P. Moreau, S.O. Døskeland, F. Anizon, L. Herfindal, A kinase inhibitor with anti-Pim kinase activity is a potent and selective cytotoxic agent towards acute myeloid leukemia, Mol. Cancer Ther. 18 (2019), https://doi.org/10.1158/1535-7163.MCT-17-1234 molcanther.1234.2017.

[26] L. Oftedal, L. Myhren, J. Jokela, G. Gausdal, K. Sivonen, S.O. Døskeland, L. Herfindal, The lipopeptide toxins anabaenolysin A and B target biological membranes in a cholesterol-dependent manner, Biochim. Biophys. Acta Biomembr. 1818 (2012) 3000–3009, https://doi.org/10.1016/j.bbamem.2012.07.015.

[27] S. Jo, J.B. Lim, J.B. Klauda, W. Im, CHARMM-GUI membrane builder for mixed bilayers and its application to yeast membranes, Biophys. J. 97 (2009) 50–58, https://doi.org/10.1016/j.bpj.2009.04.013.

[28] D.A. Case, T. Darden, T.E. Cheatham, C. Simmerling, J. Wang, R.E. Duke, R. Luo, R.C. Walker, W. Zhang, K.M. Merz, B.P. Roberts, S. Hayik, A. Roitberg, G. Seabra, J. Swails, A.W. Götz, I. Kolossváry, K.F. Wong, F. Paesani, J. Vanicek, R.M. Wolf, J. Liu, X. Wu, S.R. Brozell, T. Steinbrecher, H. Gohlke, Q. Cai, X. Ye, J. Wang, M.-J. Hsieh, G. Cui, D.R. Roe, D.H. Mathews, M.G. Seetin, R. Salomon-Ferrer, C. Sagui, V. Babin, T. Luchko, S. Gusarov, A. Kovalenko, P.A. Kollman, AMBER 12, University of California, San Francisco, 2012 (doi:citeulike-article-id:10779586).

[29] W.L. Jorgensen, J. Chandrasekhar, J.D. Madura, R.W. Impey, M.L. Klein,

Comparison of simple potential functions for simulating liquid water, J. Chem. Phys. 79 (1983) 926–935, https://doi.org/10.1063/1.445869.
[30] D.A. Case, D.S. Cerutti, T.E.I. Cheatham, T.A. Darden, R.E. Duke, T.J. Giese, H. Gohlke, A.W. Goetz, D. Greene, N. Homeyer, S. Izadi, A. Kovalenko, T.S. Lee, S. LeGrand, P. Li, C. Lin, J. Liu, T. Luchko, R. Luo, D. Mermelstein, K.M. Merz, G. Monard, H. Nguyen, I. Omelyan, A. Onufriev, F. Pan, R. Qi, D.R. Roe, A. Roitberg, C. Sagui, C.L. Simmerling, W.M. Botello-Smith, J. Swails, R.C. Walker, J. Wang, R.M. Wolf, X. Wu, L. Xiao, D.M. York, P.A. Kollman, AMBER 2017, University of California, San Francisco, 2017 (doi:citeulike-article-id:2734527).
[31] A.W. Götz, M.J. Williamson, D. Xu, D. Poole, S. Le Grand, R.C. Walker, Routine microsecond molecular dynamics simulations with AMBER on GPUs. 1. Generalized born, J. Chem. Theory Comput. 8 (2012) 1542–1555, https://doi.org/10.1021/ct200909j.
[32] H.J.C. Berendsen, J.P.M. Postma, W.F. Van Gunsteren, A. Dinola, J.R. Haak, Molecular dynamics with coupling to an external bath, J. Chem. Phys. 81 (1984) 3684–3690, https://doi.org/10.1063/1.448118.
[33] R.W. Pastor, B.R. Brooks, A. Szabo, An analysis of the accuracy of Langevin and molecular dynamics algorithms, Mol. Phys. 65 (1988) 1409–1419, https://doi.org/10.1080/00268978800101881.
[34] W.H. Gerwick, B.S. Moore, Lessons from the past and charting the future of marine natural products drug discovery and chemical biology, Chem. Biol. 19 (2012) 85–98, https://doi.org/10.1016/j.chembiol.2011.12.014.
[35] M. Costa, J. Costa-Rodrigues, M.H. Fernandes, P. Barros, V. Vasconcelos, R. Martins, Marine cyanobacteria compounds with anticancer properties: a review on the implication of apoptosis, Mar. Drugs 10 (2012) 2181–2207, https://doi.org/10.1007/978-3-319-07145-9_29.
[36] L.A. Salvador-Reyes, H. Luesch, Biological targets and mechanisms of action of natural products from marine cyanobacteria, Nat. Prod. Rep. 32 (2015) 478–503, https://doi.org/10.1039/c4np00104d.
[37] G. Kroemer, L. Galluzzi, P. Vandenabeele, J. Abrams, E.S. Alnemri, E.H. Baehrecke, M.V. Blagosklonny, W.S. El-Deiry, P. Golstein, D.R. Green, M. Hengartner, R.A. Knight, S. Kumar, S.A. Lipton, W. Malorni, G. Nuñez, M.E. Peter, J. Tschopp, J. Yuan, M. Piacentini, B. Zhivotovsky, G. Melino, Classification of cell death: recommendations of the Nomenclature Committee on Cell Death 2009, Cell Death Differ. 16 (2009) 3–11, https://doi.org/10.1038/cdd.2008.150.
[38] N. Frenkel, A. Makky, I.R. Sudji, M. Wink, M. Tanaka, Mechanistic investigation of interactions between steroidal saponin digitonin and cell membrane models, J. Phys. Chem. B 118 (2014) 14632–14639, https://doi.org/10.1021/jp5074939.
[39] M. Nishikawa, S. Nojima, T. Akiyama, U. Sankawa, K. Inoue, Interaction of digitonin and its analogs with membrane cholesterol, J. Biochem. 96 (1984) 1231–1239 http://www.ncbi.nlm.nih.gov/pubmed/6097588.
[40] S.E. Horvath, G. Daum, Lipids of mitochondria, Prog. Lipid Res. 52 (2013) 590–614, https://doi.org/10.1016/j.plipres.2013.07.002.
[41] G. van Meer, D.R. Voelker, G.W. Feigenson, Membrane lipids: where they are and how they behave, Nat. Rev. Mol. Cell Biol. 9 (2008) 112–124, https://doi.org/10.1038/nrm2330.
[42] K. Cornelio, R.A. Espiritu, Y. Todokoro, S. Hanashima, M. Kinoshita, N. Matsumori, M. Murata, S. Nishimura, H. Kakeya, M. Yoshida, S. Matsunaga, Sterol-dependent membrane association of the marine sponge-derived bicyclic peptide theonellamide a as examined by 1H NMR, Bioorg. Med. Chem. 24 (2016) 5235–5242, https://doi.org/10.1016/j.bmc.2016.08.043.
[43] R. Maget-Dana, M. Ptak, F. Peypoux, G. Michel, Pore-forming properties of iturin A, a lipopeptide antibiotic, Biochim. Biophys. Acta Biomembr. 815 (1985) 405–409, https://doi.org/10.1016/0005-2736(85)90367-0.
[44] R. Maget-Dana, I. Harnois, M. Ptak, Interactions of the lipopeptide antifungal iturin A with lipids in mixed monolayers, Biochim. Biophys. Acta Biomembr. 981 (1989) 309–314, https://doi.org/10.1016/0005-2736(89)90042-4.
[45] S.A. Cochrane, J.C. Vederas, Lipopeptides from *Bacillus* and *Paenibacillus* spp.: a gold mine of antibiotic candidates, Med. Res. Rev. 36 (2016) 4–31, https://doi.org/10.1002/med.21321.
[46] S. Dufour, M. Deleu, K. Nott, B. Wathelet, P. Thonart, M. Paquot, Hemolytic activity of new linear surfactin analogs in relation to their physico-chemical properties, Biochim. Biophys. Acta, Gen. Subj. 1726 (2005) 87–95, https://doi.org/10.1016/j.bbagen.2005.06.015.
[47] O. Lopez, M. Cócera, A. de la Maza, Influence of the level of ceramides on the permeability of stratum corneum lipid liposomes caused by a C12-alkyl betaine/sodium dodecyl sulfate mixture, Int. J. Pharm. 183 (1999) 165–173, https://doi.org/10.1016/S0927-7757(99)00092-8.
[48] T.M. Ferreira, F. Coreta-Gomes, O.H.S. Ollila, M.J. Moreno, W.L.C. Vaz, D. Topgaard, Cholesterol and POPC segmental order parameters in lipid membranes: solid state ^{1}H–^{13}C NMR and MD simulation studies, Phys. Chem. Chem. Phys. 15 (2013) 1976–1989, https://doi.org/10.1039/C2CP42738A.
[49] B.D. Madej, I.R. Gould, R.C. Walker, A parameterization of cholesterol for mixed lipid bilayer simulation within the Amber Lipid14 force field, J. Phys. Chem. B 119 (2015) 12424–12435, https://doi.org/10.1021/acs.jpcb.5b04924.
[50] M.D. Peraro, F.G. Van Der Goot, Pore-forming toxins: ancient, but never really out of fashion, Nat. Rev. Microbiol. 14 (2016) 77–92, https://doi.org/10.1038/nrmicro.2015.3.
[51] K.C. Gray, D.S. Palacios, I. Dailey, M.M. Endo, B.E. Uno, B.C. Wilcock, M.D. Burke, Amphotericin primarily kills yeast by simply binding ergosterol, Proc. Natl. Acad. Sci. U. S. A. 109 (2012) 2234–2239, https://doi.org/10.1073/pnas.1117280109.
[52] T.K. Shishido, A. Humisto, J. Jokela, L. Liu, M. Wahlsten, A. Tamrakar, D.P. Fewer, P. Permi, A.P.D. Andreote, M.F. Fiore, K. Sivonen, Antifungal compounds from cyanobacteria, Mar. Drugs 13 (2015) 2124–2140, https://doi.org/10.3390/md13042124.
[53] M. Aydin, N. Lucht, W.A. König, R. Lupp, G. Jung, G. Winkelmann, Structure elucidation of the peptide antibiotics herbicolin A and B, Liebigs Ann. Der Chemie. (11) (1985) 2285–2300, https://doi.org/10.1002/jlac.198519851117.
[54] K. Graupner, K. Scherlach, T. Bretschneider, G. Lackner, M. Roth, H. Gross, C. Hertweck, Imaging mass spectrometry and genome mining reveal highly antifungal virulence factor of mushroom soft rot pathogen, Angew. Chem. Int. Ed. 51 (2012) 13173–13177, https://doi.org/10.1002/anie.201206658.
[55] H.J. Kim, H.S. Choi, S.Y. Yang, I.S. Kim, T. Yamaguchi, J.K. Sohng, S.K. Park, J.C. Kim, C.H. Lee, B.M. Gardener, Y.C. Kim, Both extracellular chitinase and a new cyclic lipopeptide, chromobactomycin, contribute to the biocontrol activity of *Chromobacterium* sp. C61, Mol. Plant Pathol. 15 (2014) 122–132, https://doi.org/10.1111/mpp.12070.
[56] A. Afonso, F. Hon, R. Brambilla, M.S. Puar, Structure elucidation of Sch 20561, a cyclic dehydropeptide lactone - a major component of W-10 antifungal antibiotic, J. Antibiot. (Tokyo) 52 (1999) 398–406.
[57] A. Afonso, F. Hon, R. Brambilla, Structure elucidation of Sch 20562, a glucosidic cyclic dehydropeptide lactone - the major component of W-10 antifungal antibiotic, J. Antibiot. (Tokyo) 52 (1999) 383–397.
[58] E.A. Freundt, G. Winkelmann, Activity of herbicolin A against *Mycoplasma*, *Acholeplasma*, *Ureaplasma*, and *Spiroplasma* species, Antimicrob. Agents Chemother. 26 (1984) 112–114, https://doi.org/10.1128/AAC.26.1.112.
[59] J.K. Volkman, Sterols in microorganisms, Appl. Microbiol. Biotechnol. 60 (2003) 495–506, https://doi.org/10.1007/s00253-002-1172-8.
[60] V.A.C. Abreu, R.V. Popin, D.O. Alvarenga, P.D.C. Schaker, C. Hoff-Risseti, A.M. Varani, M.F. Fiore, Genomic and genotypic characterization of *Cylindrospermopsis raciborskii*: toward an intraspecific phylogenetic evaluation by comparative genomics, Front. Microbiol. 9 (2018) 1–12, https://doi.org/10.3389/fmicb.2018.00306.
[61] T.K. Shishido, J. Jokela, C.-T. Kolehmainen, D.P. Fewer, M. Wahlsten, H. Wang, L. Rouhiainen, E. Rizzi, G. De Bellis, P. Permi, K. Sivonen, Antifungal activity improved by coproduction of cyclodextrins and anabaenolysins in cyanobacteria, Proc. Natl. Acad. Sci. U. S. A. 112 (2015) 13669–13674, https://doi.org/10.1073/pnas.1510432112.
[62] S.Y. Eid, M.Z. El-Readi, M. Wink, Digitonin synergistically enhances the cytotoxicity of plant secondary metabolites in cancer cells, Phytomedicine. 19 (2012) 1307–1314, https://doi.org/10.1016/j.phymed.2012.09.002.
[63] I.R. Sudji, Y. Subburaj, N. Frenkel, A.J. García-Sáez, M. Wink, Membrane disintegration caused by the steroid saponin digitonin is related to the presence of cholesterol, Molecules. 20 (2015) 20146–20160, https://doi.org/10.3390/molecules201119682.